

基于 SLM 的股骨柄多孔结构设计与力学性能分析

曾寿金^{1,2*}, 刘广¹, 李传生¹, 叶建华¹, 李涤尘²

¹福建工程学院机械与汽车工程学院, 福建 福州 350118;

²西安交通大学机械制造系统工程国家重点实验室, 陕西 西安 710054

摘要 为了减轻传统股骨柄与股骨之间弹性模量相差较大而造成的应力遮挡效应, 采用激光选区熔化(SLM)技术制备了基于三周期极小曲面(TPMS)的多孔结构, 研究了孔隙率为 55%~75% 的 P、G、D 三种 TPMS 结构的力学性能, 并通过有限元分析评估了不同孔隙率的 P 结构股骨柄在植入股骨后的应力遮挡程度。压缩试验结果表明: 在适合骨细胞生长的孔隙率范围内, TPMS 结构的屈服强度均大于股骨的屈服强度, 满足股骨柄设计的强度要求, 并且 TPMS 结构的力学性能随孔隙率的升高而降低, 其中 P 结构降低的幅度最大。有限元分析结果表明, 在股骨柄中引入 P 结构后能够有效缓解应力遮挡效应, 有利于提高股骨柄的稳定性和使用寿命。

关键词 激光技术; 激光选区熔化; 三周期极小曲面; 多孔股骨柄; 设计; 力学性能

中图分类号 TB31; TN249

文献标志码 A

doi: 10.3788/CJL202249.0202016

1 引言

髋关节是人体中使用最频繁的承重部位之一, 很容易发生病变和损伤。目前, 针对髋关节疾病的常用治疗方法之一就是全髋关节置换术(THA)^[1], 但手术中用到的传统金属假体的弹性模量太大, 会导致应力遮挡现象发生, 进而引发假体的无菌性松动^[2]。据报道^[3], 这种假体的无菌性松动是造成全髋关节置换术失败的原因之一, 使得初次全髋关节置换术后需要进行翻修手术。

在医学领域, 通常在假体中设置合适的多孔结构, 以有效降低假体的弹性模量^[4-5]。Arabnejad 等^[6]使用一种概念化的二维晶格多孔结构来填充股骨柄, 这种设计能够在植入假体后, 使股骨应力分布得更加均匀, 减少骨吸收。Jetté 等^[7]发现采用金刚石晶格结构对股骨柄主体进行填充设计能有效降低实心假体 30% 的弹性模量, 可以减轻应力遮挡效应。Simoneau 等^[8]将假体柄部近端部分进行了不规则多孔结构填充, 并证明了该结构可以较好地分

散应力, 改善假体的受力情况。Limmahakhun 等^[9]设计了具有柱状八面体结构的多孔股骨柄, 测试后发现, 在股骨柄上合理设置多孔结构不仅可以将相对微动控制在骨长入范围内, 还可以减轻应力遮挡效应, 具有延长假体使用寿命的巨大潜力。虽然这些多孔结构应用于股骨柄后都能显著减轻应力遮挡效应, 但它们并不是最好的选择, 因为它们与人体骨组织结构存在较大差异; 此外, 这些多孔结构主要由一些棱柱组成, 棱柱之间的连接处并没有实现光滑过渡, 会造成应力集中现象, 削弱假体的性能。而基于三周期极小曲面(TPMS)的多孔结构, 其内部光滑连续, 并能通过改变函数的参数来控制多孔结构的各种特征, 为模拟人骨组织结构提供了最大的可能性^[10-12], 从而可以诱导骨生长, 增强假体与骨组织的结合, 提高假体的长期稳定性^[13-14]。Rajagopalan 等^[15]也证明了 TPMS 结构在生物学上具有天然亲和力, 这些都表明将其用于假体设计具有巨大优势, 但目前将其应用在股骨柄设计中的公开报道并不多见。

收稿日期: 2021-07-28; 修回日期: 2021-08-18; 录用日期: 2021-09-02

基金项目: 国家自然科学基金(51575110)、福建省自然科学基金(2021J011052)、福建省中小企业智能制造公共服务平台资助项目(GY-Z15127)、福建工程学院科研启动基金(GY-Z19118)

通信作者: *zengshoujin@fjut.edu.cn

激光选区熔化(SLM)技术是金属增材制造技术中的一种^[16],可以成型出具有复杂几何特征的三维零件^[17~19],且成型件的力学性能优良,在医学领域被广泛使用^[20~21],可为TPMS结构的成型提供技术支持。Zhang等^[22]采用SLM技术制备了Primitive(P)、Gyroid(G)、Diamond(D)三种TPMS结构和体心立方(BCC)结构,并证明了TPMS结构的力学性能明显优于BCC结构,其中D结构的力学性能最好。Yan等^[23]采用SLM技术制备出G和D两种TPMS结构,并评估了TPMS结构的可制造性和力学性能;结果表明:TPMS结构的计算机断层扫描(CT)重建模型与原始模型高度一致,并且TPMS结构的弹性模量和孔隙率可以根据人体骨骼水平进行调整,从而减少或避免了应力遮挡效应。Ma等^[24]发现:采用SLM制造的G结构支架具有优异的力学性能,可以模拟人体骨骼;G结构具有良好的流动性,对通道中间的流体具有加速作用,有利于养分的输送。Abueidda等^[25]通过实验和仿真两种方法研究了P、IWP和Neovius三种TPMS结构的力学性能,结果表明,P结构具有最小的弹性模量,能为减

少植入手的应力遮挡提供最大可能性。因此,本文选择P、G、D三种具有骨植入应用潜力的TPMS结构,并利用SLM技术制备出了具有不同孔隙率的样件,对其力学性能进行研究;在确定适合设计股骨柄的结构类型后,通过有限元分析评估了该结构填充的股骨柄在植入后对股骨的应力遮挡情况,旨在减轻应力遮挡效应的同时为骨细胞生长提供空间,增强股骨柄的长期稳定性,延长股骨柄的使用寿命。

2 材料与方法

2.1 TPMS结构的建模方法

极小曲面是任何一点的平均曲率为零的曲面。TPMS是一个在三维空间的三个方向上周期性无限延伸的极小曲面,它的表达方式有很多种,其中水平集近似方程的表达方式可能是最常用的^[26]。水平集方程是满足方程 $\Phi(x,y,z)=C$ 的三角函数的组合,其中函数 $\Phi(x,y,z)=C$ 描述了在等值C(水平集常数)处计算的表面。本文选择了三个常用的TPMS曲面,即G、D、P结构。它们的水平集方程可以描述为

$$\Phi_P(x,y,z) = \cos(\omega x) + \cos(\omega y) + \cos(\omega z) = C, \quad (1)$$

$$\Phi_G(x,y,z) = \cos(\omega x)\sin(\omega y) + \cos(\omega y)\sin(\omega z) + \cos(\omega z)\sin(\omega x) = C, \quad (2)$$

$$\begin{aligned} \Phi_D(x,y,z) = & \sin(\omega x)\sin(\omega y)\sin(\omega z) + \cos(\omega x)\sin(\omega y)\sin(\omega z) + \sin(\omega x)\cos(\omega y)\sin(\omega z) + \\ & \sin(\omega x)\sin(\omega y)\cos(\omega z) = C, \end{aligned} \quad (3)$$

式中: x 、 y 、 z 为空间坐标; $\omega=2\pi/l$, l 为单位晶胞的长度。此外, C 能够控制曲面的形状以及相应的TPMS结构的孔隙率。接下来以P结构为例说明TPMS结构的建模过程。建模过程如图1所示,使用软件Wolfram Mathematica通过定义函数方程 $-C \leq \Phi(x,y,z) \leq C$ 建立两个不同的等值面,并将单位空间内两等值面之间的部分定义为实体,从而实现多孔结构模型的构建。

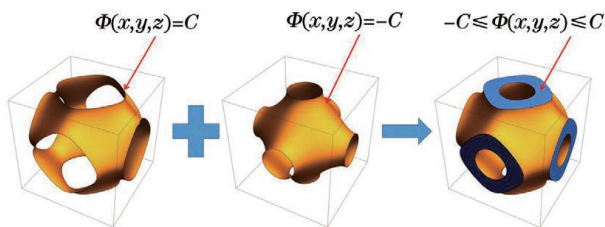


图1 P结构的建模过程

Fig. 1 Modeling process of P structure

为了方便多孔样件的设计,有必要对多孔结构的设计参数及孔隙率进行研究。本文通过设置一系

列间隔为0.1的C值,建立了相应的三维模型,并计算得到了其孔隙率。拟合得到的C值与孔隙率之间的数学关系如图2所示。可以发现,TPMS结构的C值与孔隙率 p_u 之间近似满足线性关系。

2.2 TPMS结构样件的设计及SLM成型

根据多孔结构在股骨柄中的功能特性,股骨柄中的多孔结构应满足以下要求:1)多孔结构应具有一定的功能性,即能促进骨长入。多孔结构的孔径、孔隙率对骨细胞的生长有很明确的影响。据报道^[27~29],当孔径为0.2~1.2 mm、孔隙率大于50%时,多孔结构适合骨细胞迁移、附着和增殖。Ma等^[30]对G型TPMS结构的研究表明,大孔径的多孔结构具有高的细胞生长速率,更有利于细胞迁移生长。这是因为渗透性在细胞增殖中起主要作用,而较大的孔径使多孔支架具有更高的渗透性,从而促进骨骼修复。因此,为使股骨柄植入股骨后,细胞能快速迁移生长,股骨柄在较短时间内就能具有良好的长期稳定性,在设计TPMS结构时,应首先

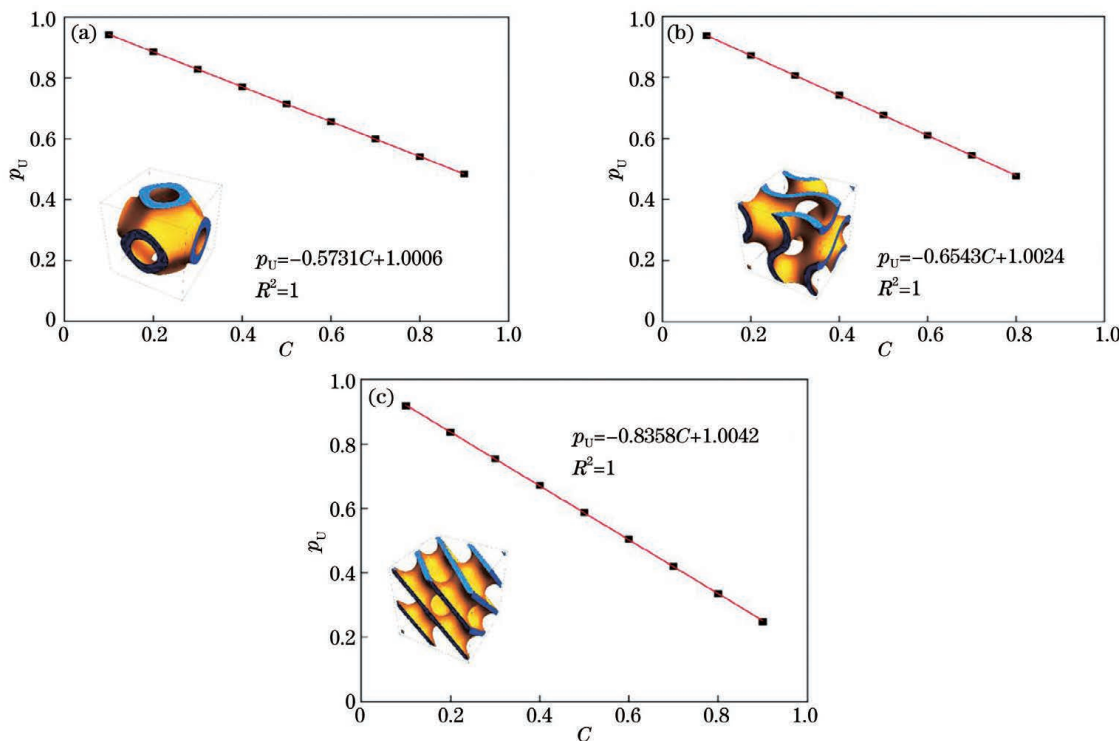


图2 TPMS结构的C值与孔隙率之间的关系。(a)P结构;(b)G结构;(c)D结构

Fig. 2 Relationship between C value and porosity in TPMS structure. (a) P structure; (b) G structure; (c) D structure

确保TPMS结构的孔径较大,并在适合细胞生长的孔径范围内。2)多孔结构应具有足够的强度,就屈服强度而言,多孔结构的屈服强度需要大于股骨的屈服强度,这样才能保证股骨柄在植入后,其中的多孔结构在人体日常活动的载荷下不发生变形,避免股骨柄失效。因此,TPMS结构的孔隙率不宜太高,因为太高的孔隙率会显著降低TPMS结构的力学性能。3)多孔结构需要能准确地制备出来,保证

设计出的多孔结构与制造出的多孔结构保持高度一致,从而为以上两点奠定基础。因此,多孔结构的设计需要考虑成型设备的制造精度。为保证样件的成型质量,多孔结构的设计须满足以下约束条件:薄板的最小厚度大于0.2 mm,最小孔径大于0.2 mm。根据上述约束条件,本文选取的样件的具体设计参数如表1所示。多孔结构的壁厚和孔径参数定义如图3所示。

表1 TPMS结构样件的设计参数

Table 1 Design parameters of TPMS structural samples

Type (size)	Parameter	Design 1	Design 2	Design 3	Design 4	Design 5
P (unit size: 3 mm; sample size: 12 mm× 12 mm×12 mm)	Porosity /%	55	60	65	70	75
	Constant C	0.79	0.70	0.61	0.53	0.44
	Pore size /mm	0.63	0.76	0.88	0.97	1.02
	Thickness /mm	0.67	0.58	0.50	0.42	0.34
G (unit size: 4 mm; sample size: 16 mm× 16 mm×16 mm)	Porosity /%	55	60	65	70	75
	Constant C	0.69	0.62	0.54	0.46	0.39
	Pore size /mm	0.81	0.90	0.99	1.08	1.17
	Thickness /mm	0.65	0.58	0.50	0.42	0.36
D (unit size: 4 mm; sample size: 16 mm× 16 mm×16 mm)	Porosity /%	55	60	65	70	75
	Constant C	0.54	0.48	0.42	0.36	0.30
	Pore size /mm	0.89	0.96	1.02	1.08	1.14
	Thickness /mm	0.51	0.46	0.40	0.34	0.28

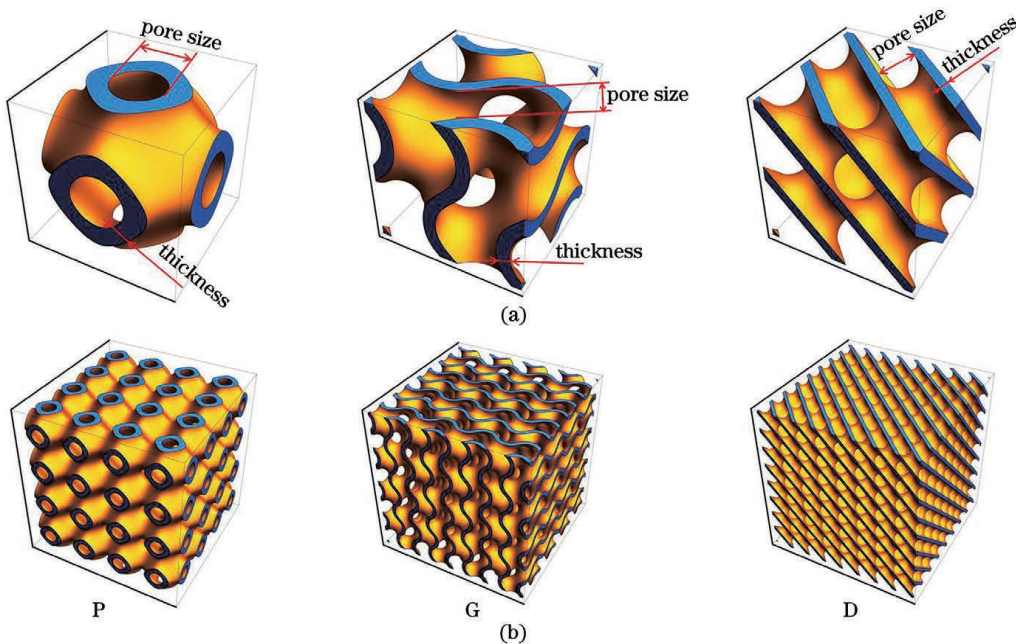


图3 TPMS多孔结构的参数定义及样本模型。(a)壁厚及孔径;(b)样本模型

Fig. 3 Parameter definitions and sample models of TPMS structures. (a) Wall thickness and pore size; (b) sample model

实验中使用的金属粉末为 Ti-6Al-4V 合金粉，其在不同倍率下的扫描电镜(SEM)图像如图 4 所示。粉末颗粒接近球形且表面光滑，具有良好的流动性。

该粉末的粒度分布为 3~50 μm，平均粒度约为 20 μm，粉末的化学成分如表 2 所示。实验前，粉末在 80 °C 下真空干燥 8 h 以上。

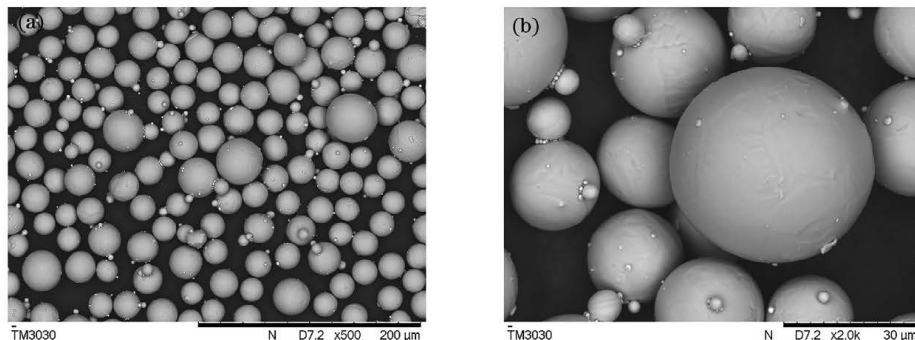


图4 Ti-6Al-4V 粉末形貌

Fig. 4 Morphologies of Ti-6Al-4V powder

表2 Ti-6Al-4V 粉末的化学成分

Table 2 Chemical composition of Ti-6Al-4V powder

Element	Mass fraction /%
Al	6.0~6.5
V	3.5~4.5
O	≤0.10
N	≤0.03
C	≤0.08
H	≤0.012
Fe	≤0.25
Ti	Bal.

成型设备采用德国 SLM 公司生产的 SLM-125HL 打印机，激光器为 IPG 光纤激光器，功率为 400 W，采用的工艺参数如下：激光功率 275 W，扫描间距 0.12 mm，扫描速度 1100 mm/s，铺粉厚度 30 μm。制造完成后，采用电火花线切割机切下样品。为减小残留粉末对成型件力学行为的影响，采用超声波清洗机对其进行清洗。

2.3 力学性能测试

利用 DNS300 电子万能试验机进行室温压缩测试，恒定加载速度为 2 mm/min。在垂直于打印方向上对样品进行测试，试样放置在加载板的中心，以确保均匀加载并消除错位引起的力矩。压缩停止

后,计算机生成位移-载荷数据文件,数据采集完毕。

2.4 生物力学仿真

股骨柄近端因应力遮挡效应而发生的骨质丢失最为严重,将假体近端设计为多孔结构,可以利用多孔结构弹性模量小的特性来改善应力传递不均的问题,从而降低应力遮挡效应。此外,假体近端与股骨接触较为紧密,将假体近端设计为多孔结构有助于骨长入,提高股骨柄植入后的长期稳定性。因此,本研究团队将股骨柄假体的近端设计为上述初步优选后的多孔结构,示意图如图5(a)所示。为了分析股骨柄假体植入后的应力遮挡情况,对股骨、实心股骨柄和多孔股骨柄分别进行有限元仿真模拟。由于股骨的工况多种多样,受力情况较为复杂,为了便于说明,采用具有代表性的双足静止站立受载模型,这是股骨受到的最基本的载荷。对于静力分析来说,这是一种简单有效的载荷。将股骨按照正常站立位放置,在股骨头最高处施加载荷。Bergmann等^[31]的研究表明,日常常见活动中股骨头上的最大载荷为体重的3.35倍。志愿者的体重为63 kg,所以合力大小设置为2100 N,受力模型如图5(b)所示。假体柄部与股骨的接触设置为摩擦接触,摩擦因子为0.4^[32]。此外,为了减少计算机的计算时间,与其他学者的设置方法一样^[9],将实验部分得到的多孔结构弹性模量赋给实体,以模拟多孔结构。股骨的赋值在Mimics中采用经验公式(4)和(5)来设置^[33]。

$$\rho = 1.067 HU + 131, \quad (4)$$

$$E = 0.004\rho^{2.01}, \quad (5)$$

式中: HU 为CT值; ρ 为材料的密度; E 为弹性模量。

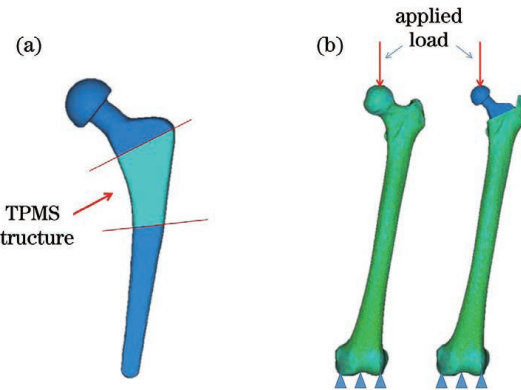


图5 多孔股骨柄的设计及边界条件设置。(a)多孔股骨柄;(b)边界条件

Fig. 5 Design of porous femoral stem and boundary conditions setting. (a) Porous femoral stem; (b) boundary condition

3 结果与讨论

3.1 样件成型效果

图6为SLM制备的TPMS多孔结构样件及其表面形貌。可以看出,多孔结构样件表面无明显缺陷,所有样件都是完整且连续的,轮廓规则、清晰,样件表面出现的粉末黏附现象也较轻微,样件的外形成型效果较好。此外,为了表示TPMS结构的设计模型与实际样件之间的差别,对样件的孔径及壁厚

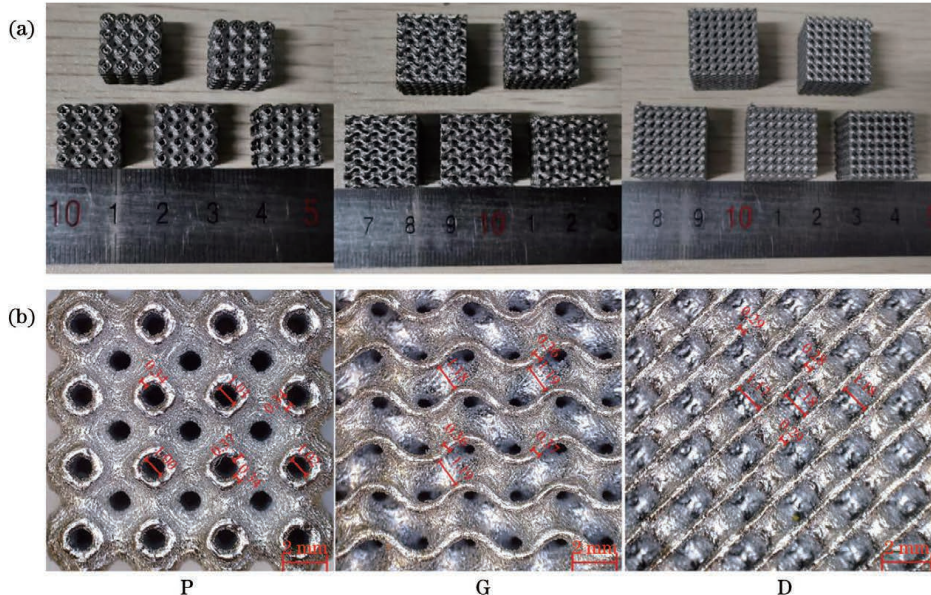


图6 采用SLM技术制备的TPMS多孔样件及其表面形貌。(a)TPMS多孔样件;(b)表面形貌

Fig. 6 Porous TPMS samples prepared by selective laser melting (SLM) and their surface topographies. (a) Porous TPMS samples; (b) surface topographies

尺寸进行了测量。由于孔隙率为75%的样件的壁厚比较接近SLM设备成型的约束条件,出现样件与模型相差较大的可能性最大,具有一定的代表性,因此选取其表面形貌中轮廓清晰的部分作为测量对象,测量结果标在图6(b)中。从图6(b)可以看出:就TPMS结构的壁厚而言,P结构有一条边的壁厚存在加厚的情况,但从数值上看,它与模型的壁厚相差得并不算太大,其他三条边上的壁厚都与模型的壁厚相符;而G和D结构虽然并未出现较为明显的厚薄不均的现象,但也与模型存在着微小偏差。另外,对于TPMS结构的孔径而言,P和G这两种结构的样件与模型之间具有较好的一致性,相比于这两种结构,D结构表现出的偏差则稍显偏大,但与设计的孔径尺寸相比,这些偏差并不算大,是可以接受

的。总体而言,TPMS结构的样件与设计模型相差不大,整体成型效果较好。

3.2 多孔样件的力学性能分析

3.2.1 弹性模量和屈服强度分析

数据采集完成后,采用Origin软件绘制压缩应力-应变曲线,结果如图7所示。观察图7可以发现,在曲线的线性弹性阶段之前存在非线性阶段,这是因为样件的端面与平台并不完全平行,在这期间,样件与压头逐渐建立起完整的接触^[24]。每种结构的弹性模量由线性弹性阶段的斜率来定义。此外,该曲线并未表现出明显的屈服行为,因此以0.2%塑性应变下的应力作为屈服准则,用以获得屈服强度。屈服强度的具体数值记录于表3。人体股骨的弹性模量通常为15.4~18.7 GPa,屈服强度为

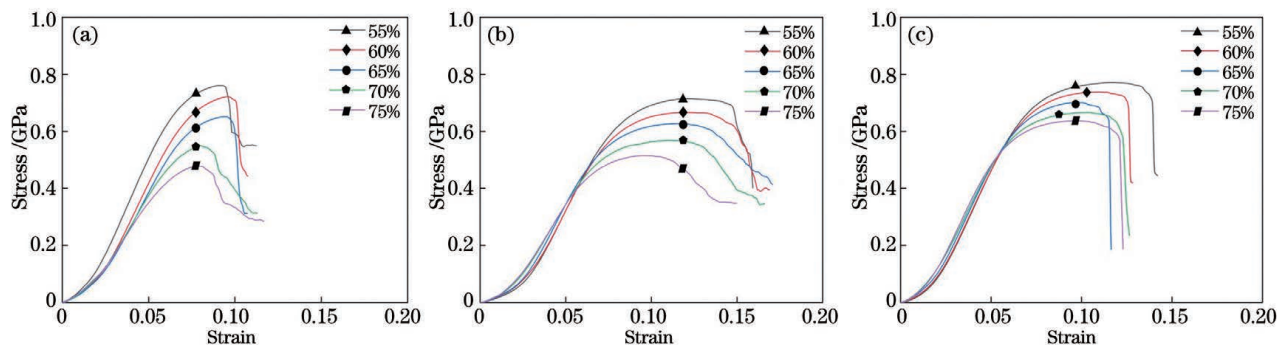


图7 TPMS多孔样件的压缩应力-应变曲线。(a)P结构;(b)G结构;(c)D结构

Fig. 7 Compressive stress-strain curves of TPMS porous samples. (a) P structure; (b) G structure; (c) D structure

表3 计算得到的TPMS多孔样件的弹性模量和屈服强度

Table 3 Calculated elastic modulus and yield strength of TPMS porous samples

Type	Designed porosity /%	Thickness /mm	Elastic modulus /GPa	Yield strength /MPa
P	55	0.67	13.33	638.89
	60	0.58	12.29	601.02
	65	0.50	11.22	558.74
	70	0.42	10.22	472.21
	75	0.34	9.19	414.44
G	55	0.65	11.32	583.87
	60	0.58	11.18	537.51
	65	0.50	10.89	504.33
	70	0.42	9.82	465.29
	75	0.36	9.50	427.67
D	55	0.51	13.44	603.14
	60	0.46	12.98	598.41
	65	0.40	12.87	571.64
	70	0.34	12.52	538.27
	75	0.28	12.28	527.12

179~209 MPa。分析表3可以发现,采用SLM技术制备的多孔样件的弹性模量在9.19~13.44 GPa之间,与人体股骨的弹性模量相近,屈服强度在414~639 MPa之间,高于人体股骨的屈服强度^[34],说明满足假体设计的强度要求。孔隙率与力学性能的关系如图8所示,从图中可以清晰地看出,P、G、D三种结构的弹性模量和屈服强度都随着孔隙率的增大而降低,与典型多孔材料的规律相同。此外还可

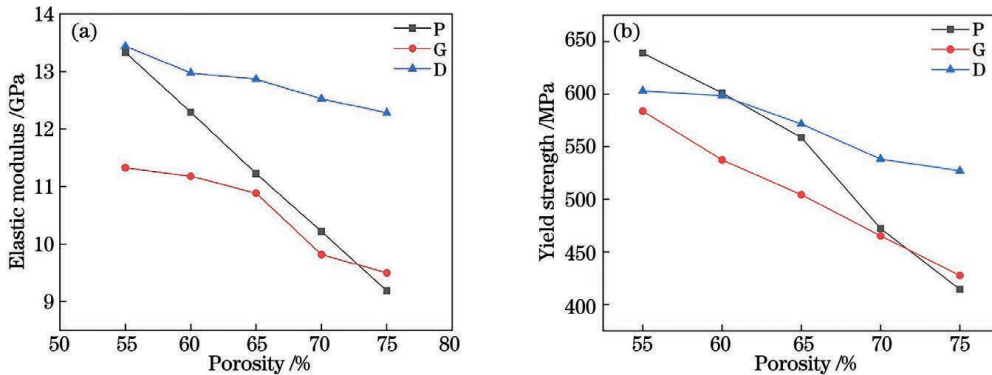


图8 TPMS多孔样件孔隙率与力学性能之间的关系。(a)弹性模量;(b)屈服强度

Fig. 8 Relationship between porosity and mechanical properties of TPMS porous samples. (a) Elastic modulus; (b) yield strength

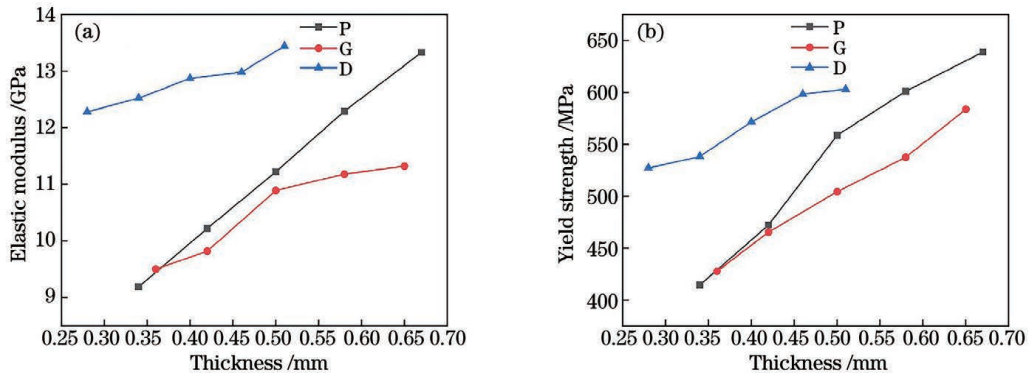


图9 TPMS多孔结构壁厚与力学性能的关系。(a)弹性模量;(b)屈服强度

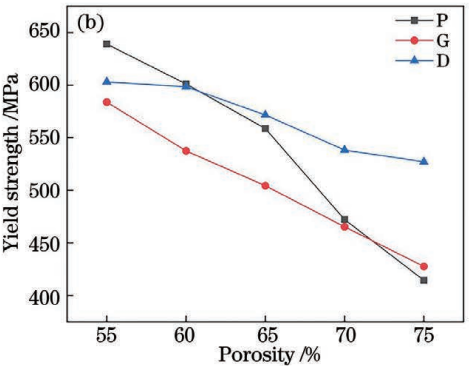
Fig. 9 Relationship between thickness and mechanical properties of TPMS porous structures. (a) Elastic modulus; (b) yield strength

3.2.2 多孔结构设计参数与力学性能之间的关系

为了更好地指导个性化假体多孔结构的设计,需要获得多孔结构设计参数与力学性能之间的关系。首先基于实验结果,通过Gibson-Ashby理论模型来拟合力学性能与多孔结构孔隙率之间的数学模型^[35],再将其与多孔结构设计部分得出的设计参数与孔隙率的关系式进行串联,得到TPMS结构的预测公式。Gibson-Ashby理论模型的数学表达式为

$$\frac{E}{E_s} = C_1 \left(\frac{\rho}{\rho_s} \right)^{n_1}, \quad (6)$$

以看出,在高孔隙率下,D结构表现出了最好的力学性能。图9为TPMS多孔结构的壁厚与力学性能之间的关系,从图中可以看出:随着壁厚增加,TPMS多孔结构的弹性模量和屈服强度都增大;当壁厚相同时,D结构的力学性能依旧比其他两种结构更好,并且D结构是三种结构中力学性能受壁厚影响最小的结构,表明该结构比较稳定;P结构是三种结构中受壁厚影响最大的结构。



度时,拉伸和弯曲变形主导的结构的相应 n 值分别为 $n=1$ 和 $n=1.5$, n 的其他值表现为混合变形模

式。TPMS 结构的相对密度与力学性能之间的关系如图 10 所示。

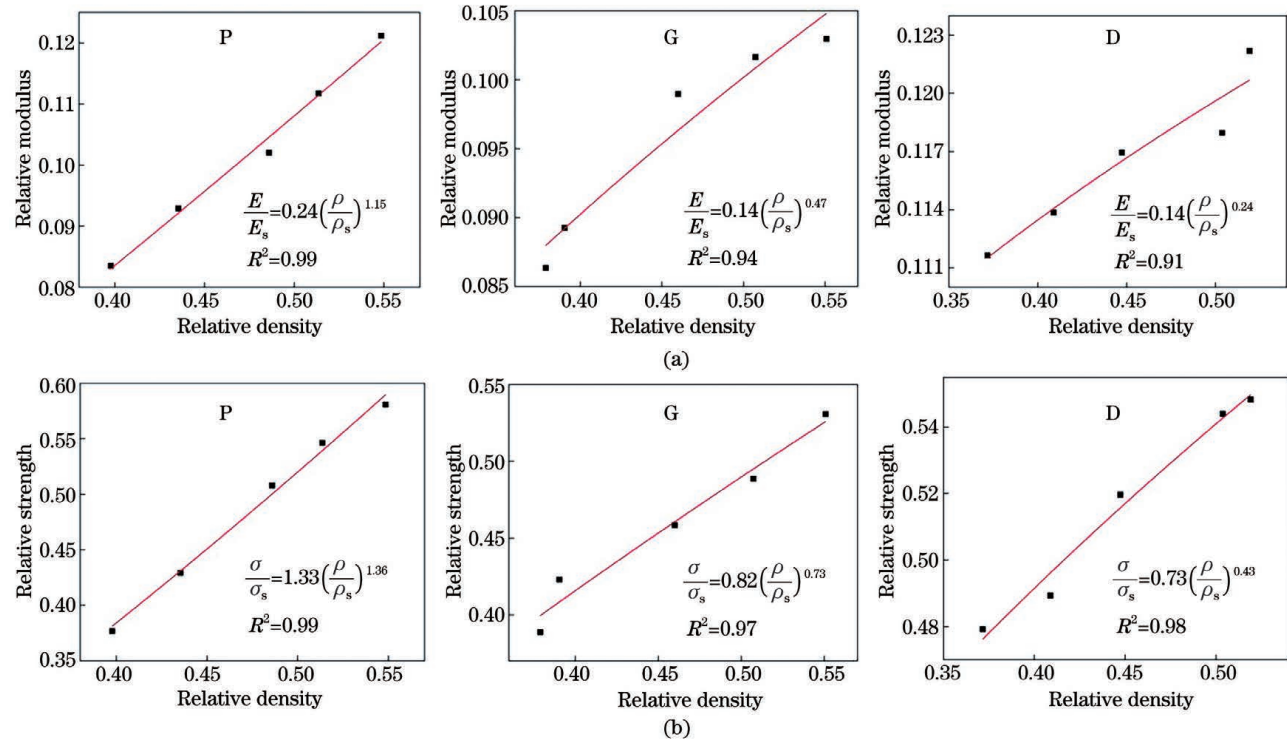


图 10 相对密度与力学性能之间的关系。(a) 相对密度与相对模量的关系;(b) 相对密度与相对强度的关系

Fig. 10 Relationship between relative density and mechanical properties. (a) Relationship between relative density and relative modulus; (b) relation between relative density and relative strength

由图 10 可知,多孔样件的力学性能拟合程度较好。将力学性能与设计参数、孔隙率的等式关联后,得到了 TPMS 多孔结构的设计参数与力学性能的关系式,如(8)~(13)式所示。

P 结构:

$$E = 0.24(0.5731C - 0.0006)^{1.15} E_s, \quad (8)$$

$$\sigma = 1.33(0.5731C - 0.0006)^{1.36} \sigma_s. \quad (9)$$

G 结构:

$$E = 0.14(0.6543C - 0.0024)^{0.47} E_s, \quad (10)$$

$$\sigma = 0.82(0.6543C - 0.0024)^{0.73} \sigma_s. \quad (11)$$

D 结构:

$$E = 0.14(0.8358C - 0.0042)^{0.24} E_s, \quad (12)$$

$$\sigma = 0.73(0.8358C - 0.0042)^{0.43} \sigma_s. \quad (13)$$

从弹性模量的角度来看,只有 P 结构表现出了以拉伸为主的变形模式,G、D 结构均表现为混合变形模式,但三种结构都未表现出以弯曲为主的变形模式。据报道^[36],与弯曲支配的多孔结构相比,拉伸支配的多孔结构通常具有更好的力学性能。这表明,相比其他多孔结构,TPMS 结构具有更好的力学性能。从 n 的具体数值来看,本文与 Bobbert

等^[37]的研究存在一定差异,主要表现在 D 和 G 这两种结构上。这可能是由于 D 和 G 的内部结构复杂,悬垂特征较多,在成型满足细胞生长的这种小尺寸多孔样件时,样件内部容易出现大量挂渣,从而导致样件内部可能存在堵粉现象。Abou-Ali 等^[38]的研究结果也证实了这一点。P 结构的内部构造简单,受设计尺寸的影响较小,能较好地还原设计模型的尺寸和性能。

此外,G 和 D 结构的 n 值较小,说明它们的力学性能受相对密度变化的影响很小。然而,在实际应用中,特别是在定制化股骨柄的设计中,由于每个人的骨骼结构和力学性能各不相同,这就导致需要设计不同力学性能的假体去匹配相应的股骨;但多孔结构由于受成型设备制造精度和人骨细胞生长要求的制约,其设计空间并不大,并且与以往多孔结构的优选思路不同的是,单纯追求高孔隙率和高力学性能的最佳多孔结构是不适用的。在满足假体强度要求的条件下,最大化减轻应力遮挡效应才是本文追求的主要目标。因此,在设计定制化股骨柄时,设计者更需要的是一种适应性更高的多孔结构,这种结构能在有限的设计范围内,既满足股骨柄设计的

强度要求,又能大幅调节股骨柄的力学性能,以便与不同宿主骨的力学性能相匹配,最大程度降低应力遮挡效应,提高假体的稳定性和使用寿命。因此,G结构和D结构并不适合用于设计股骨柄。

综上所述,在满足假体强度要求的前提下,相较于G和D这两种结构,P结构在可制造性和调节力学性能方面的能力都表现出更大的综合优势,是股骨柄多孔结构设计的良好选择。为了进一步研究P

结构用于多孔股骨柄时的具体效果,对P结构股骨柄进行了生物力学仿真。

3.3 有限元模型验证

股骨的仿真结果如图11所示,可见,应力较大的部位主要出现在股骨颈处、上1/3段的股骨干处以及下1/3段的股骨干处。这些部位正是在正常人体解剖结构中骨质明显增厚、密度增大,以增加强度和抵抗较大负荷的部位,符合正常股骨中的应力分布。

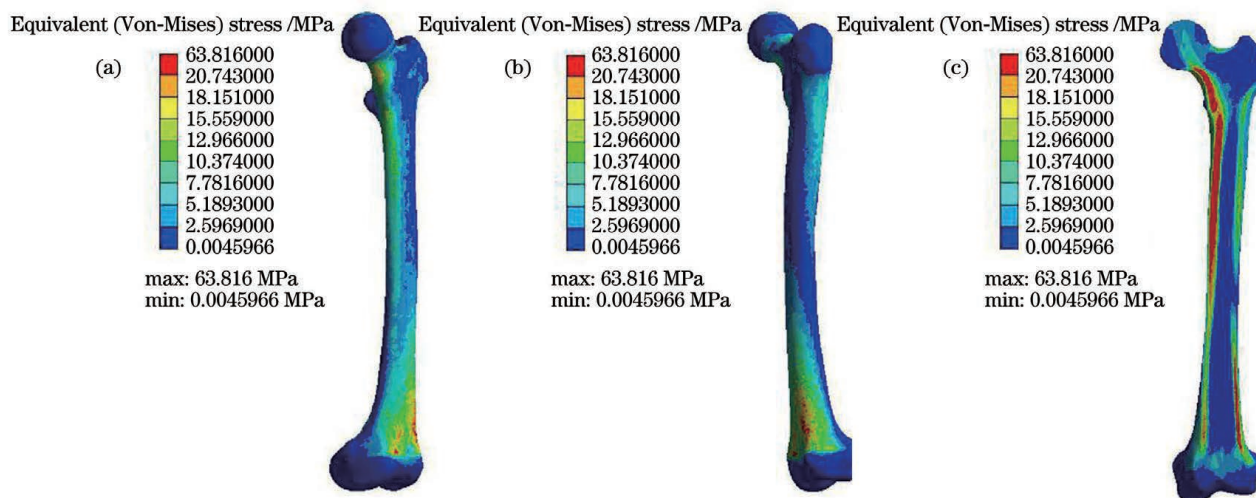


图11 股骨的应力分布。(a)股骨内侧应力分布;(b)股骨外侧应力分布;(c)股骨内部应力分布

Fig. 11 Stress distributions in femur. (a) Stress distribution in medial femur; (b) stress distribution in lateral femur; (c) stress distribution inside the femur

植入实心股骨柄后,有限元分析模型的验证如图12所示。从图中可以看出,本研究得到的力-位移曲线与Jetté等^[39]的研究结果很接近,具有较好的一致性。由此可见,本文使用的有限元分析模型是正确的,可用于后续分析。

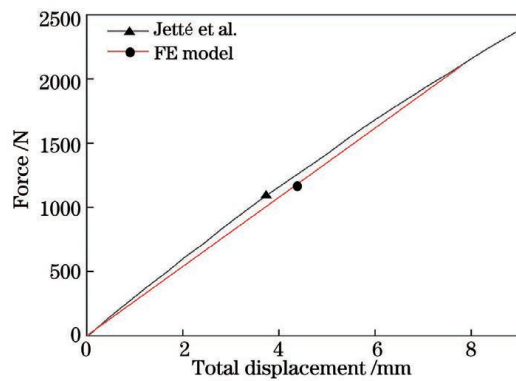


图12 有限元分析模型的验证

Fig. 12 Verification of finite element (FE) analysis model

3.4 仿真结果分析

根据上面得到的结论,将孔隙率为55%~75%的P结构设计为股骨柄的多孔结构,并对其进行有限元分析。分析结果显示,5种孔隙率的P结构股

骨柄的应力峰值按孔隙率由大到小排列分别为91.64, 91.59, 91.53, 91.46, 91.39 MPa, 均小于多孔结构的屈服强度,满足股骨柄设计的强度要求。

为了解THA手术前后股骨应力的变化,采用Gruen分区方法对股骨的应力进行分析。Gruen分区示意图和股骨手术前后的应力分布如图13所示,可以看出:术后股骨的应力相比术前均存在一定程度的应力遮挡效应;但相较于实心股骨柄,P结构股骨柄在THA手术后的应力分布得到了明显改善,尤其是股骨近端。这表明股骨柄在引入多孔结构后,可以有效缓解应力遮挡效应。此外,通过这7组模型的应力云图可以看出,Gruen 1~6区的颜色变化不明显,Gruen 7区却有明显的不同。这表明THA手术后应力遮挡程度最大的地方发生在Gruen 7区域,与以往的研究结果一致^[40-41]。

为了解不同孔隙率的P结构股骨柄植入后股骨的应力遮挡程度,采用应力遮挡率进行定量分析。应力遮挡率的计算公式为

$$\psi = \left(1 - \frac{\sigma_p}{\sigma_o}\right) \times 100\%, \quad (14)$$

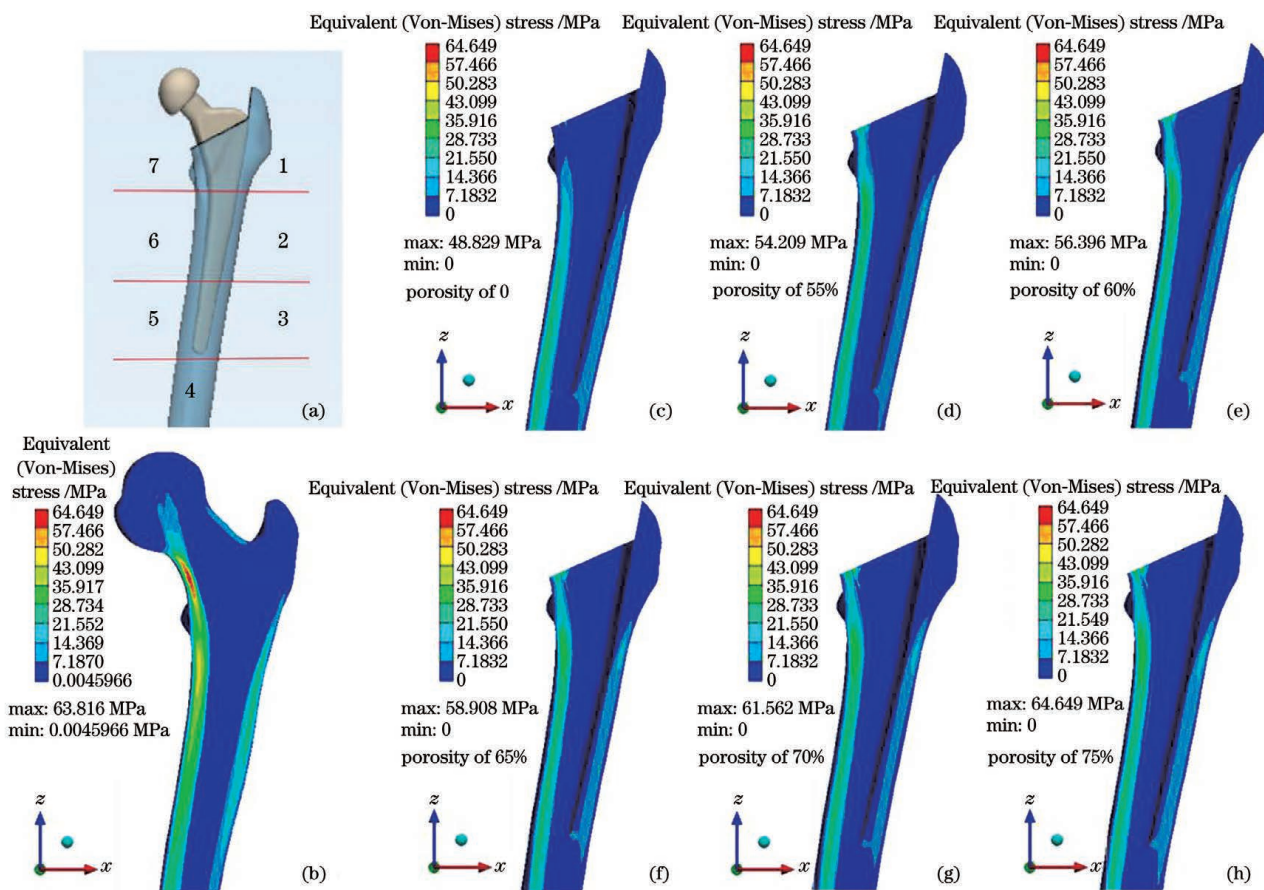


图 13 Gruen 分区示意图以及股骨手术前后的应力分布。(a)Gruen 分区示意图;(b)术前股骨的应力分布;(c)~(h)术后股骨的应力分布

Fig. 13 Gruen zoning diagram and stress distributions in femur before and after surgery. (a) Gruen zoning diagram; (b) stress distribution in femur before surgery; (c)–(h) stress distribution in femur after surgery

式中: ψ 为应力遮挡率; σ_p 为植入假体后股骨中的应力; σ_0 为植入假体前股骨中的应力。

THA 手术后,股骨出现应力遮挡效应最大的区域为 Gruen 7 区域,通过分析 Gruen 7 区域的应力遮挡率,就能得到多孔股骨柄降低应力遮挡的能力;因此,本文只需计算 Gruen 7 区的应力遮挡率。为了保证数据的准确性,在每根股骨的 Gruen 7 区,沿着骨内侧线选择 10 个相应位置,求取其应力平均值,并将应力平均值作为最终的应力数据,将其代入(14)式计算出应力遮挡率。计算后可知:植入实心股骨柄引起的应力遮挡率达到了 87.55%,而植入 P 结构孔隙率为 55%、60%、65%、70% 和 75% 的股骨柄引起的应力遮挡率分别为 58.79%、57.07%、55.16%、53.19% 和 50.93%。相较于实心股骨柄,多孔结构的引入至少使应力遮挡率降低了 28.76 个百分点,其中孔隙率为 75% 的 P 结构降低的应力遮挡程度最高,使应力遮挡率降低了 36.62 个百分点。这表明,对于 P 结构而言,通过调节孔隙率还能使

应力遮挡率进一步降低。综上所述,孔隙率为 75% 的 P 结构最适合用于股骨柄的多孔结构设计。

4 结 论

为缓解植入传统股骨柄后引起的应力遮挡效应,本研究团队选择对生物细胞亲和力更好的 TPMS 结构作为股骨柄的多孔结构,通过力学性能测试实验和有限元仿真得出了以下结论:

- 利用优化的工艺参数制备出的 TPMS 多孔结构样件成型效果良好。通过压缩试验发现,在骨生长需求和 SLM 设备的制造约束范围内,三种常见 TPMS 多孔结构的力学性能均能够满足股骨柄的使用要求。

- 对比 G 结构和 D 结构,P 结构在可制造性和调节力学性能方面都表现出较大的综合优势,是一种更适合用于股骨柄设计的多孔结构。此外,依据 Gibson-Ashby 理论模型计算得出了设计参数与多孔结构力学性能之间的关系式,可以通过设计参数

来预测多孔结构的力学性能,用于指导股骨柄多孔结构的设计。

3) 有限元分析结果表明,在日常常见活动载荷下,P结构股骨柄中的应力峰值并未超过多孔材料的屈服强度,因此该结构能够用于股骨柄多孔结构的设计。此外,在股骨柄中引入P结构后,相应股骨中的应力分布得到了显著改善,能有效缓解应力遮挡效应。孔隙率为75%的P结构是最优选择,能够降低应力遮挡率,提高假体植入后的长期稳定性和使用寿命。

参 考 文 献

- [1] Alonso-Rasgado T, Del-Valle-Mojica J F, Jimenez-Cruz D, et al. Cement interface and bone stress in total hip arthroplasty: relationship to head size[J]. *Journal of Orthopaedic Research*, 2018, 36(11): 2966-2977.
- [2] Ridzwan M I Z, Shuib S, Hassan A Y, et al. Problem of stress shielding and improvement to the hip implant designs: a review[J]. *Journal of Medical Sciences*, 2007, 7(3): 460-467.
- [3] Sundfeldt M, Carlsson L V, Johansson C B, et al. Aseptic loosening, not only a question of wear: a review of different theories[J]. *Acta Orthopaedica*, 2006, 77(2): 177-197.
- [4] Limmahakun S, Oloyede A, Sitthiseripratip K, et al. Stiffness and strength tailoring of cobalt chromium graded cellular structures for stress-shielding reduction[J]. *Materials & Design*, 2017, 114: 633-641.
- [5] Wieding J, Wolf A, Bader R. Numerical optimization of open-porous bone scaffold structures to match the elastic properties of human cortical bone[J]. *Journal of the Mechanical Behavior of Biomedical Materials*, 2014, 37: 56-68.
- [6] Arabnejad S, Johnston B, Tanzer M, et al. Fully porous 3D printed titanium femoral stem to reduce stress-shielding following total hip arthroplasty[J]. *Journal of Orthopaedic Research*, 2017, 35(8): 1774-1783.
- [7] Jetté B, Brailovski V, Dumas M, et al. Femoral stem incorporating a diamond cubic lattice structure: design, manufacture and testing[J]. *Journal of the Mechanical Behavior of Biomedical Materials*, 2018, 77: 58-72.
- [8] Simoneau C, Terriault P, Jetté B, et al. Development of a porous metallic femoral stem: design, manufacturing, simulation and mechanical testing[J]. *Materials & Design*, 2017, 114: 546-556.
- [9] Limmahakun S, Oloyede A, Chantarapanich N, et al. Alternative designs of load-sharing cobalt chromium graded femoral stems[J]. *Materials Today Communications*, 2017, 12: 1-10.
- [10] Ma S H, Song K L, Lan J, et al. Biological and mechanical property analysis for designed heterogeneous porous scaffolds based on the refined TPMS[J]. *Journal of the Mechanical Behavior of Biomedical Materials*, 2020, 107: 103727.
- [11] Song K L, Wang Z H, Lan J, et al. Porous structure design and mechanical behavior analysis based on TPMS for customized root analogue implant [J]. *Journal of the Mechanical Behavior of Biomedical Materials*, 2021, 115: 104222.
- [12] Wang S, Shi Z A, Liu L L, et al. The design of Ti6Al4V Primitive surface structure with symmetrical gradient of pore size in biomimetic bone scaffold [J]. *Materials & Design*, 2020, 193: 108830.
- [13] Murr L E. Open-cellular metal implant design and fabrication for biomechanical compatibility with bone using electron beam melting[J]. *Journal of the Mechanical Behavior of Biomedical Materials*, 2017, 76: 164-177.
- [14] Takemoto M, Fujibayashi S, Neo M, et al. Mechanical properties and osteoconductivity of porous bioactive titanium[J]. *Biomaterials*, 2005, 26(30): 6014-6023.
- [15] Rajagopalan S, Robb R A. Schwarz meets Schwann: design and fabrication of biomorphic and durataxic tissue engineering scaffolds[J]. *Medical Image Analysis*, 2006, 10(5): 693-712.
- [16] Li S C, Mo B, Xiao G, et al. Microstructure characteristics and their influence factors during laser additive manufacturing of metal materials[J]. *Laser & Optoelectronics Progress*, 2021, 58(1): 100007.
- 李时春,莫彬,肖罡,等.金属材料的激光增材制造微观组织结构特征及其影响因素[J].*激光与光电子学进展*,2021,58(1):100007.
- [17] Gu D D, Zhang H M, Chen H Y, et al. Laser additive manufacturing of high-performance metallic aerospace components[J]. *Chinese Journal of Lasers*, 2020, 47(5): 050002.
- 顾冬冬,张红梅,陈洪宇,等.航空航天高性能金属材料构件激光增材制造[J].*中国激光*,2020,47(5):0500002.
- [18] Duan S Q, Liu T T, Liao W H, et al. Research on forming quality of overhanging round hole by selective laser melting[J]. *Chinese Journal of Lasers*, 2018,

- 45(4): 0402007.
- 段声勤, 刘婷婷, 廖文和, 等. 悬垂圆孔激光选区熔化成形质量研究[J]. 中国激光, 2018, 45(4): 0402007.
- [19] Zhang B, Cao Y, Wang L, et al. Anisotropy of body-centered-cubic porous structures by selective laser melting[J]. Chinese Journal of Lasers, 2017, 44(8): 0802005.
- 张博, 曹毅, 王玲, 等. 选区激光熔化体心立方多孔结构的各向异性[J]. 中国激光, 2017, 44(8): 0802005.
- [20] Yao Y S, Tang J P, Wang J, et al. Forming technology and properties of 316L stainless steel by selective laser melting[J]. Laser & Optoelectronics Progress, 2021, 58(1): 0114006.
- 姚燕生, 唐建平, 汪俊, 等. 选区激光熔化316L不锈钢成形工艺与性能研究[J]. 激光与光电子学进展, 2021, 58(1): 0114006.
- [21] Guo Q F, Zhang Z, Huang L J, et al. Effects of pulsed laser on surface quality and deformation of selective laser melted Ti6Al4V titanium alloy [J]. Laser & Optoelectronics Progress, 2020, 57(21): 211404.
- 郭庆丰, 张政, 黄李杰, 等. 脉冲激光对选区激光熔融Ti6Al4V钛合金表面质量及变形量的影响[J]. 激光与光电子学进展, 2020, 57(21): 211404.
- [22] Zhang L, Feih S, Daynes S, et al. Energy absorption characteristics of metallic triply periodic minimal surface sheet structures under compressive loading [J]. Additive Manufacturing, 2018, 23: 505-515.
- [23] Yan C Z, Hao L, Hussein A, et al. Ti-6Al-4V triply periodic minimal surface structures for bone implants fabricated via selective laser melting[J]. Journal of the Mechanical Behavior of Biomedical Materials, 2015, 51: 61-73.
- [24] Ma S, Tang Q, Feng Q X, et al. Mechanical behaviours and mass transport properties of bone-mimicking scaffolds consisted of gyroid structures manufactured using selective laser melting[J]. Journal of the Mechanical Behavior of Biomedical Materials, 2019, 93: 158-169.
- [25] Abueidda D W, Bakir M, Abu Al-Rub R K, et al. Mechanical properties of 3D printed polymeric cellular materials with triply periodic minimal surface architectures[J]. Materials & Design, 2017, 122: 255-267.
- [26] Gandy P J F, Bardhan S, MacKay A L, et al. Nodal surface approximations to the P, G, D and I-WP triply periodic minimal surfaces[J]. Chemical Physics Letters, 2001, 336(3/4): 187-195.
- [27] Ki C S, Park S Y, Kim H J, et al. Development of 3-D nanofibrous fibroin scaffold with high porosity by electrospinning: implications for bone regeneration [J]. Biotechnology Letters, 2008, 30(3): 405-410.
- [28] Lin C Y, Kikuchi N, Hollister S J. A novel method for biomaterial scaffold internal architecture design to match bone elastic properties with desired porosity [J]. Journal of Biomechanics, 2004, 37(5): 623-636.
- [29] Stamboulis A G, Boccaccini A R, Hench L L. Novel biodegradable polymer/bioactive glass composites for tissue engineering applications[J]. Advanced Engineering Materials, 2002, 4(3): 105-109.
- [30] Ma S, Tang Q, Han X X, et al. Manufacturability, mechanical properties, mass-transport properties and biocompatibility of triply periodic minimal surface (TPMS) porous scaffolds fabricated by selective laser melting[J]. Materials & Design, 2020, 195: 109034.
- [31] Bergmann G, Deuretzbacher G, Heller M, et al. Hip contact forces and gait patterns from routine activities [J]. Journal of Biomechanics, 2001, 34(7): 859-871.
- [32] Pettersen S H, Wik T S, Skallerud B. Subject specific finite element analysis of implant stability for a cementless femoral stem[J]. Clinical Biomechanics, 2009, 24(6): 480-487.
- [33] Rho J Y, Hobatho M C, Ashman R B. Relations of mechanical properties to density and CT numbers in human bone [J]. Medical Engineering & Physics, 1995, 17(5): 347-355.
- [34] Zhang X Z, Leary M, Tang H P, et al. Selective electron beam manufactured Ti-6Al-4V lattice structures for orthopedic implant applications: current status and outstanding challenges[J]. Current Opinion in Solid State and Materials Science, 2018, 22(3): 75-99.
- [35] Ashby M F. The properties of foams and lattices[J]. Philosophical Transactions of the Royal Society A, 2006, 364(1838): 15-30.
- [36] Kadkhodapour J, Montazerian H, Darabi A C, et al. The relationships between deformation mechanisms and mechanical properties of additively manufactured porous biomaterials [J]. Journal of the Mechanical Behavior of Biomedical Materials, 2017, 70: 28-42.
- [37] Bobbert F S L, Lietaert K, Eftekhari A A, et al. Additively manufactured metallic porous biomaterials based on minimal surfaces: a unique combination of topological, mechanical, and mass transport properties [J]. Acta Biomaterialia, 2017, 53: 572-584.
- [38] Abou-Ali A M, Al-Ketan O, Lee D W, et al. Mechanical behavior of polymeric selective laser

- sintered ligament and sheet based lattices of triply periodic minimal surface architectures [J]. Materials & Design, 2020, 196: 109100.
- [39] Jetté B, Brailovski V, Simoneau C, et al. Development and *in vitro* validation of a simplified numerical model for the design of a biomimetic femoral stem [J]. Journal of the Mechanical Behavior of Biomedical Materials, 2018, 77: 539-550.
- [40] Alkhatib S E, Tarlochan F, Mehboob H, et al. Finite element study of functionally graded porous femoral stems incorporating body-centered cubic structure [J]. Artificial Organs, 2019, 43(7): E152-E164.
- [41] Yamako G, Janssen D, Hanada S, et al. Improving stress shielding following total hip arthroplasty by using a femoral stem made of β type Ti-33.6Nb-4Sn with a Young's modulus gradation [J]. Journal of Biomechanics, 2017, 63: 135-143.

Porous Structure Design and Mechanical Properties Analysis of Femoral Stem Based on Selective Laser Melting

Zeng Shoujin^{1,2*}, Liu Guang¹, Li Chuansheng¹, Ye Jianhua¹, Li Dichen²

¹ School of Mechanical & Automotive Engineering, Fujian University of Technology, Fuzhou, Fujian 350118, China;

² State Key Laboratory for Manufacturing Systems Engineering, Xi'an Jiaotong University, Xi'an, Shaanxi 710054, China

Abstract

Objective The hip joint is one of the most frequently used load-bearing parts of the human body, which is at risk of lesions and injuries. Presently, total hip arthroplasty (THA) is a common treatment method for hip disorders. However, the elastic modulus of the traditional metal prosthesis used in surgery is extremely large, which leads to stress shielding and results in aseptic loosening of the prosthesis. This is one of the main reasons of THA failure. In the medical field, porous structures are often used in the prosthesis to reduce its elastic modulus. Therefore, various porous structures are used in the femoral stem, such as diamond structure, body centered cubic structure, and columnar octahedral structure. The introduction of these structures can reduce the stress shielding effect. However, these structures are not the best choice because they are extremely different from the human bone tissue structure. Moreover, these porous structures are mainly composed of prisms. There is no smooth transition between the prisms, which causes stress concentration and weakens the performance of the prosthesis. Based on the triply periodic minimal surface (TPMS), this study evaluates a design method of porous structure of femoral stem prosthesis, which can effectively reduce its elastic modulus and alleviate the stress shielding effect. Moreover, the porous structure based on TPMS has a smooth and continuous interior, good mechanical properties, and natural affinity in biology. Furthermore, several features of the porous structure can be precisely controlled by changing the parameters of the function, which has provided the greatest possibility for simulating the human bone tissue structure. This will be beneficial in inducing bone growth, enhancing the combination of prosthesis and bone tissue, improving the long-term stability of the prosthesis after implantation, and extending the service life of the femoral stem. The design method and research results of this study are expected to provide a new idea for improving the performance of porous femoral stems.

Methods This study analyzed the porous structure design method based on TPMS. Using the relationship between the design parameters of TPMS structure and porosity, three-dimensional models of P, G, and D structures with porosity of 55%-75% were established. Then, the corresponding Ti6Al4V titanium alloy samples were prepared using selective laser melting (SLM) technology, and their forming quality was characterized. Furthermore, the compression experiment was conducted on the sample, and the effects of wall thickness and porosity on the elastic modulus and yield strength of the TPMS structure were evaluated. The types of porous structures suitable for the femoral stem were selected. Finally, the structures with different porosities were filled in the femoral stem, and the stress shielding rate of these femoral stems after implantation was calculated by finite element analysis. Its ability to alleviate the stress shielding effect was evaluated.

Results and Discussions In the analysis of the porous structure design method for femoral stem prosthesis, the

function of the porous structure in the femoral stem and manufacturing precision constraints of equipment were considered (Table 1). Compression experiments showed that the mechanical properties of these structures can meet the service requirements of the femoral stem (Table 3). Moreover, the P structure can be adjusted through the wall thickness and porosity, thereby greatly adjusting its mechanical properties (Figs. 8, 9). The relationship between structural design parameters and mechanical properties of the porous structure is calculated using Gibson-Ashby's theoretical model (Formulas 8–13), which can achieve the purpose of using design parameters to predict mechanical properties of the porous structure. The simulation analysis results of femoral stress before and after THA show that the P structure femoral stem can significantly improve the stress distribution of the corresponding femur and alleviate the stress shielding effect (Fig. 13).

Conclusions To alleviate the stress shielding effect caused by the implantation of the traditional femoral stem, the TPMS structure with better affinity for the biological cell is selected as the porous structure of the femoral stem. The TPMS structure sample can be formed better through SLM technology. The compression test results show that the mechanical properties of the three common TPMS porous structures can meet the requirements on the use of femoral stems within the constraints of bone growth and SLM equipment manufacturing. Compared with the G and D structures, the P structure shows greater comprehensive advantage in manufacturability and ability to adjust. It is a porous structure more suitable for the design of the femoral stem. The results of finite element analysis show that the peak stress of the P structure femoral stem does not exceed the yield strength of porous materials under common daily active loads, which proves that the application of P structure in the femoral stem can meet the needs of daily activities. Moreover, after the introduction of P structure in the femoral stem, the stress distribution of the corresponding femur is significantly improved, which can effectively alleviate the stress shielding effect. Among these, the P structure with a porosity of 75% is the best, which can reduce the stress shielding rate by 41.83 percentage points. This is beneficial in improving the long-term stability and service life of the prosthesis after implantation.

Key words laser technique; selective laser melting; triply periodic minimal surface; porous femoral stem; design; mechanical properties